Purinergic Signalling (2015) 11:229–238
DOI 10.1007/s11302-015-9448-5

ORIGINAL ARTICLE

Roles of the lateral fenestration residues of the $P2X_4$ receptor that contribute to the channel function and the deactivation effect of ivermectin

Chao Gao[1] · Qiaqia Yu[1] · Huijuan Xu[2] · Longmei Zhang[1] · Jingxin Liu[1] · Yanling Jie[2] · Wenbo Ma[2] · Damien S. K. Samways[3] · Zhiyuan Li[2,4]

Received: 29 December 2014 / Accepted: 18 March 2015 / Published online: 7 April 2015

Abstract P2X receptors are cation-permeable ion channels gated by extracellular adenosine triphosphate (ATP). Available crystallographic data suggest that ATP-binding ectodomain is connected to the transmembrane pore domain by three structurally conserved linker regions, which additionally frame the lateral fenestrations through which permeating ions enter the channel pore. The role of these linker regions in relaying the conformational change evoked by ATP binding of the ectodomain to the pore-forming transmembrane domain has not been investigated systematically. Using $P2X_4R$ as our model, we employed alanine and serine replacement mutagenesis to determine how the side chain structure of these linker regions influences gating. The mutants Y54A/S, F198A/S, and W259A/S all trafficked normally to the plasma membrane of transfected HEK293 cells but were poorly responsive to ATP. Nevertheless, the function of the F198A/S mutants could be recovered by pretreatment with the known positive allosteric modulator of $P2X_4R$, ivermectin (IVM), although the IVM sensitivity of this mutant was significantly impaired relative to wild type. The functional mutants Y195A/S, F200A/S, and F330A/S exhibited ATP sensitivities identical to wild type, consistent with these side chains playing no role in ATP binding. However, Y195A/S, F200A/S, and F330A/S all displayed markedly changed sensitivity to the specific effects of IVM on current deactivation, suggesting that these positions influence allosteric modulation of gating. Taken together, our data indicate that conserved amino acids within the regions linking the ectodomain with the pore-forming transmembrane domain meaningfully contribute to signal transduction and channel gating in P2X receptors.

Key words $P2X_4$ receptor · Ivermectin · ATP · Deactivation · Fenestration domain

Abbreviations

TM	Transmembrane segment
IVM	Ivermectin
EC_{50}	Concentration for half-maximal response
τ_{off}	Deactivation time constant
I_{max}	The maximal amplitude of the current activated by ATP
HEK293	Human embryonic kidney 293

Introduction

P2X receptors (P2XRs) are ligand-gated nonselective cation channels activated by extracellular adenosine triphosphate (ATP) [1] and composed of seven receptor subunits ($P2X_{1-7}$) that associate, as either homo- or heterotrimeric channels [2]. These receptors play important roles in the nervous system [3], in which they can mediate and modulate fast synaptic transmission [4–8]. Different subtypes distribute differently as $P2X_4Rs$ are widely expressed in the superior cervical ganglion, brain, hippocampus, and pancreatic islet cells [9–12].

✉ Zhiyuan Li
li_zhiyuan@gibh.ac.cn

1 School of Life Sciences, University of Science and Technology of China, Hefei, Anhui 230027, China

2 Key Laboratory of Regenerative Biology, Guangzhou Institute of Biomedicine and Health, Chinese Academy of Sciences, Guangzhou, Guangdong 510530, China

3 Department of Biology, Clarkson University, 8 Clarkson Avenue, Potsdam, NY 13699, USA

4 Guangzhou Institute of Biomedicine and Health, Chinese Academy of Sciences, 190 Kai Yuan Avenue, Science Park, Guangzhou, China

Several P2XR-targeted drugs may play roles in the regulation of different P2XRs. The macrocylic lactone ivermectin (IVM) has been shown to potentiate ATP-gated currents mediated by $P2X_4R$ [13] and, more recently, the human form of $P2X_7R$ [14]. In clinical medicine, IVM is widely used in humans and animals as an antihelmintic agent for the treatment of parasitic diseases such as onchocerciasis (river blindness) [15]. Here, IVM causes membrane hyperpolarization and muscle paralysis [16] by activating glutamate-gated chloride channels in the nerves and muscles of the parasite. IVM has dramatic effects on the ATP-activated current of $P2X_4R$. The ATP-activated currents of $P2X_4R$ are dramatically affected by IVM, which increases the maximal current amplitude in the presence of saturating ATP and slows the rate of current deactivation after washout of ATP [13].

In common with all P2XRs, each functional $P2X_4R$ homomer is comprised of three subunits, with each subunit containing two transmembrane domains, intracellular -NH_2 and -COOH termini, and a large ectodomain [2]. The ectodomain can be divided into the upper vestibule, the central vestibule, and the extracellular vestibule, the latter of which lies directly adjacent to the pore-forming transmembrane domain [17]. The ectodomain is connected to the transmembrane domain by three linker regions that also serve to frame three fenestrations that are now known to be the primary point of access for ions into the extracellular vestibule and pore domain (Fig. 1a and b) [18–21]. The positioning of these linker regions between the ligand-binding ectodomain and the pore-forming transmembrane domain favor their playing a key role in signal transduction and channel gating, and yet despite this, there has been no direct effort to determine confirms this. A number of bulky side chain-bearing residues are present in the linker regions that are conserved throughout the P2XR family, including Tyr^{54}, Tyr^{195}, Phe^{198}, Phe^{200}, Trp^{259}, and Phe^{330} (Fig. 1a and b). We predicted that these might be important in stabilizing the interaction between the ectodomain and pore-forming domain and that reduction of side chain volume by substitution to alanine or serine might be expected to retard signal transduction and gating of the $P2X_4R$ channel. Furthermore, based on previous evidence that residues lining the fenestrations regulated IVM sensitivity in $P2X_4$ [18], we predicted that the allosteric effects of this drug on $P2X_4R$ gating might be impacted by amino acid substitutions introduced into this region. Thus, we studied the effects of these mutants on the ATP-induced current in both the absence and the presence of IVM.

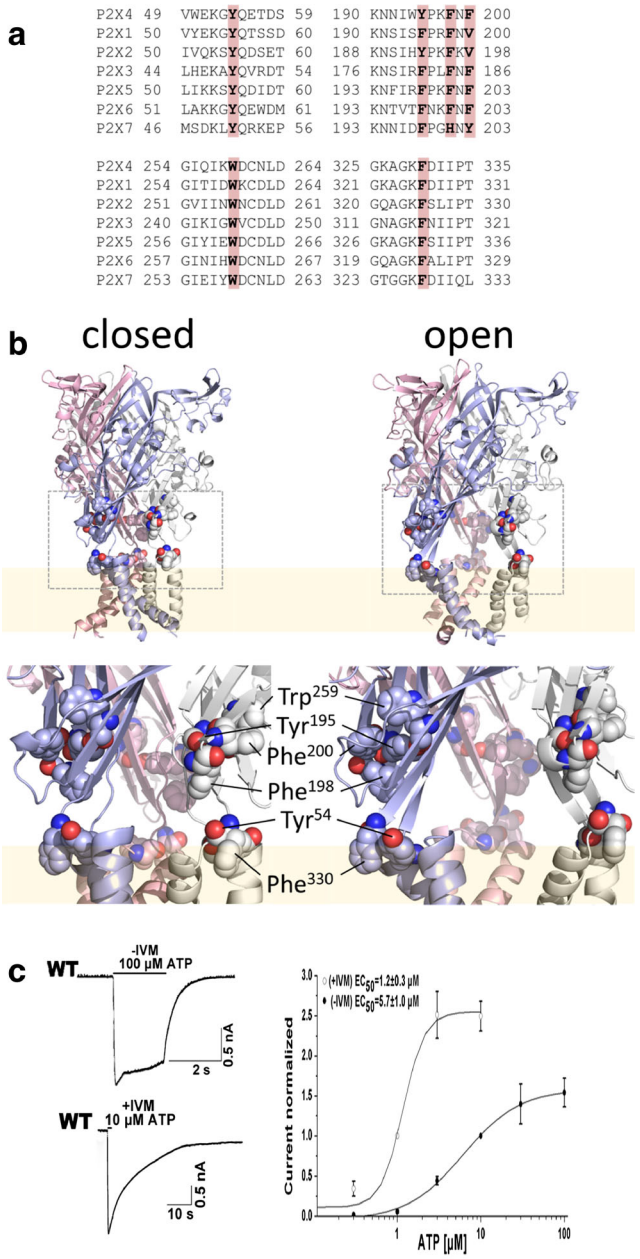

Fig. 1 Structure of fenestration aromatic residues and the ATP-induced current in HEK293 cells expressing the WT $P2X_4R$. **a** Conserved aromatic residues with large side chains in the fenestration domain (indicated by *gray areas*). **b** The models of the $rP2X_4R$ are shown in the open or closed state, and the TM domains are shown in *pink*. The fenestration domain is shown in the *dashed box*. The model shows the position of the aromatic residues. **c** Example record showing the peak current activated by ATP and the effects of IVM on the peak amplitude and deactivation time of the currents induced by ATP (in this and the following figures, the traces show experimental records, and *black bars* indicate the duration of agonist application for 1–2 s). Concentration dependence of ATP on the peak amplitude of current responses by the WT $P2X_4$ receptor in the absence (n=15, closed symbols) and presence of 3 μM IVM (n=7, open symbols)

Materials and methods

Channel constructs Rat $P2X_4$ ($rP2X_4$) clones were kindly provided by Dr. Terrance M. Egan (Saint Louis University). The rat $P2X_4$ receptor construct was used as a template for the production of plasmids containing mutations of conserved aromatic residues to alanine and serine. Point mutations were

introduced using the KOD-Plus-Mutagenesis Kit (TOYOBO, Japan) according to the manufacturer's instructions. Primers for cloning and mutagenesis were synthesized by Invitrogen (Life Technologies, USA). The phenylalanine residues at positions 198, 200, and 330; the tyrosine residues at positions 54 and 195; and the tryptophan residue at position 259 were mutated to alanine and serine. The production of the correct mutations and the absence of coding errors in the $P2X_4$ mutant constructs were verified by DNA sequencing (Automated ABI Sequencing Service, Life Technologies, USA). cDNAs were propagated in *Escherichia coli* DH5α, and the plasmids were purified using a TaKaRa MiniBest Plasmid Purification Kit (TaKaRa, Japan).

Cell culture and transfection Experiments were performed on human embryonic kidney 293 cells (HEK293 cells), which were grown in Dulbecco's modified Eagle's medium (D-MEM) supplemented with Glutamax (Invitrogen, USA), 10 % fetal bovine serum (HyClone, USA), 50 U/ml penicillin, and 50 μg/ml streptomycin in a humidified 5 % CO_2 atmosphere at 37 °C. Cells treated with trypsin were cultured in six-well plates for 24–48 h until reaching 60 %–80 % confluence before transfection. The expression vectors containing the cDNA for the wild-type and mutant $P2X_4$ receptors were transiently coexpressed together with enhanced green fluorescent protein in HEK293 cells using Effectence Transfection Reagent (QIAGEN, USA). The 4 μl of enhancer, 10 μl of effectence, 1 μg of $P2X_4$ receptor cDNA, and 1 μg of GFP cDNA were used for each transfection following the manufacturer's instructions. The plasmid encoding GFP was co-transfected to aid the visual identification of transfected cells for electrophysiological recording experiments. After 8 h of incubation, the transfection mixture was replaced with D-MEM and cultured for 24–48 h prior to whole-cell recording experiments.

Electrophysiological recordings Whole-cell currents were measured at room temperature from cells held at −60 mV using the perforated-patch, whole-cell, voltage-clamp technique. Whole-cell recordings were made with low-resistance (2−5 MΩ) borosilicate glass electrodes, which were pulled from borosilicate glass using a Flaming Brown Horizontal puller (P-97, Sutter Instruments, Novato, CA). The electrodes were filled with 200 μg/ml amphotericin B dissolved in an intracellular solution of the following composition (in mM): 130 Cs-methanesulfonate, 24 CsCl, 1 $MgCl_2$, 1 $CaCl_2$, and 10 HEPES. The dishes with cell cultures were continuously perfused with an extracellular solution of the following composition (in mM): 154 NaCl, 1 $MgCl_2$, 1 $CaCl_2$, 10 glucose, and 10 HEPES, adjusted to pH 7.3 with 1 M NaOH. All solutions were maintained at pH 7.3–7.4 and 300–328 mOsm/L. All chemicals were purchased from Sigma. In all experiments, solutions containing ATP or IVM were applied with a fast gravity-driven perfusion system consisting of an RSC-200 Rapid Solution Changer (Biologic, Claix, France). Movements of the glass tube array and solution application were controlled by protocols in the pClamp 10.0 software. Successive applications were separated by 2–5 min to minimize receptor desensitization. An Axonpatch 200B amplifier was controlled by pClamp 10.0 software via a Digidata 1440A interface board (Axon Instruments) for all recordings. Data were filtered at 2 kHz and digitized at 5 kHz.

Confocal microscopy Transiently transfected HEK293 cells with the wild-type (WT) receptor and its mutants were plated onto poly-L-lysine-coated coverslips. At 24 h after transfection, the cells were fixed for 15 min in ice-cold 4 % paraformaldehyde (pH 7.4), permeabilized with 0.5 % Triton X-100 in PBS for 15 min, and incubated in blocking buffer (1 % BSA, PBS pH 7.5) for 1 h to block nonspecific antibody binding. The cells were then incubated with blocking buffer containing primary antibody (anti-$P2X_4$ antibody, 1:1,000, Sigma, USA) at 4 °C overnight or at room temperature for 2 h. Afterward, the cells were incubated with secondary antibody (Goat Anti-Rabbit IgG-HRP, 1:2000, sigma, USA) for 30 min at room temperature. Finally, the coverslips containing transfected cells were covered with anti-fade mounting medium (Beyotime, China) to prevent fluorescence fading. The localization of the receptors in cells was examined by laser-scanning confocal microscopy (Zeiss 710 NLO, Germany). Images were collected using a 40× oil immersion objective.

Data analysis Dose–response data points were fitted by a Hill equation using a nonlinear curve-fitting program that calculated the EC_{50} and Hill coefficient values of the resulting curves (SigmaPlot version 10.0, SPSS Inc.). ATP was repeatedly applied at 1- to 2-min intervals usually with the following sequence of concentrations, 0.3, 1, 10, 3, 10, 30, 10, and 100 μM. All responses were relative to the 1 or 10 μM response. The equation was $y=A_2+(A_1-A_2)/[1+(x/EC_{50})^{nH}]$, where y was the maximum amplitude of the current evoked by a given concentration of ATP (normalized in all cases), A_2 was the maximum current amplitude, A_1 was the minimum current amplitude, EC_{50} was the agonist concentration that produced 50 % of the maximal response, n_H was the Hill coefficient, and x was the concentration of ATP. Concentration−response relationships for the effects of IVM on potentiation and deactivation were fitted by a Hill equation (SigmaPlot version 10.0, SPSS Inc.) as follows, $I_{IVM}=I_{Ctrl}+a[IVM]^{nH}/\{[IVM]^{nH}+EC_{50}{}^{nH}\}$, where I_{IVM} was I_{max} in response to 10 μM ATP at a given concentration of IVM, I_{Ctrl} was I_{max} in response to 10 μM ATP in the absence of IVM or incubated in 0.1 μM IVM, a was the maximal fold increase in I_{max} induced by IVM, [IVM] was the concentration of IVM, n_H was the Hill coefficient, and EC_{50} was the concentration of IVM that gave a half-maximal response. The kinetics of the

current decay evoked by washing out the agonists was fitted to a two-exponential function [$y=A_1 \exp(-t/\tau_1)+A_2 \exp(-t/\tau_2)$) using the program CLAMPFIT 10.2 (Axon Instruments), and the derived time constant was labeled τ_{off}. A_1 and A_2 are the relative amplitudes of the first and second exponential, respectively, and τ_1 and τ_2 are the corresponding time constants. All the numerical values in the text are reported as the means± S.E.M. for *n* cells, and significant differences were determined by using Student's *t* test. The graphical representations of the protein structure were performed using PyMOL software (DeLano Scientific LLC, USA), and the models were got from the Brookhaven Protein Data Bank (4DW1 for the zfP2X$_4$R in the ATP-bound open state and 4DW0 for the receptor in the apo-closed state).

Results

ATP- and IVM-sensitivity of wild-type P2X$_4$R Whole-cell current recordings from HEK293 cells expressing wild-type P2X$_4$R were made during repetitive (every 3 min) stimulation with 2-s pulses of 10/100 μM ATP in the presence and absence of IVM. Consistent with other work [22], we determined the EC_{50} for ATP activation of P2X$_4$R to be 5.7± 1.0 μM (Fig. 1c). Also consistent with previous studies, IVM was observed to increase the amplitude of the ATP-gated current and delay the deactivation time course after wash out of ATP [22]. In our hands, the peak amplitude of the ATP-induced current was increased approximately twofold in the presence of 3 μM IVM. We estimated the EC_{50} for ATP activation in the presence of 3 μM IVM to be 1.2± 0.3 μM, representative of an approximately fivefold increase in ATP sensitivity. The deactivation time constant (τ_{off}) for the decline in ATP-gated current upon wash out of the drug was significantly prolonged after treatment with 3 μM IVM for 5 min (from τ_{off}=0.4±0.02 s to 29±2.3 s).

Effect of linker region substitutions on ATP-dependent gating of P2X$_4$R Scanning alanine- and serine-mutagenesis was employed to determine whether conserved aromatic residues in the linker regions connecting the ecto- and transmembrane domains were important for channel function. Alanine and serine substitutions were introduced at positions Tyr^{54}, Tyr^{195}, Phe^{198}, Phe^{200}, Trp^{259}, and Phe^{330} (Fig. 1a). Tyr^{54} (Phe^{330}) was located in the interface between TM1 and β_1 (TM2 and β_{14}). Tyr^{195}, Phe^{198}, and Phe^{200} formed a random coil between β_8 and β_9, and Trp^{259} was located in β_{11} (Fig. 1b). Whole-cell recordings were used to measure the channel activity after these mutants were transfected into HEK293 cells. Mutation of Tyr^{195}, Phe^{200}, and Phe^{330} to both alanine and serine yielded functional receptors when expressed in HEK293 cells (Fig. 2a). Consistent with these residues being located relatively distant from the ATP binding domain, their EC_{50}s for ATP activation were not significantly different from wild type (Fig. 2b, Table 1). The mutants, Y54A/S, F198A/S, and W259A/S, were unresponsive to even high concentrations of ATP (up to 1–3 mM) (Fig. 2a, Table 1). To investigate whether this was due to an impairment of protein trafficking to the plasma membrane, we monitored the expression pattern of the mutants in HEK293 cells using immunofluorescence imaging (Fig. 3a). Similar to the WT control, all three mutants demonstrated substantial plasma membrane localization, suggesting normal packaging and trafficking. Further evidence that these mutants were expressed on the plasma membrane was revealed with IVM, which successfully revealed ATP-gated currents for F198 mutants (Fig. 3b, c, d, and e).

Taken together, these results suggest that mutation of side chains in this region has a profound impact on ATP gating, as would be predicted given the positions of the linkers between the ligand binding and pore-forming domains. This conclusion is supported by three pieces of evidence. First, those mutants that were functional showed normal ATP EC_{50} values. Second, not even very high concentrations of ATP could evoke currents through Y54A/S, F198A/S, and W259A/S mutants. Third, ATP-evoked currents could only be observed for F198A/S mutants after treatment with the known allosteric gating modulator, IVM.

Effect of linker region substitutions on IVM-sensitivity of P2X$_4$R gating Our data suggested that one residue, Phe^{198}, was important for normal P2X$_4$R channel gating, and that two others, Tyr^{54} and Trp^{259}, might contribute also. Previous studies had shown that IVM-modulated P2X$_4$R gating in the presence of ATP, and so we wished to test the hypothesis that mutation of residues in the linker regions might impact the sensitivity of the channel to such allosteric modulation. For the mutants F198A/S, we noted that the currents recovered in the presence of IVM had a much more rapid deactivation time course than the WT ATP-gated current in the presence of IVM. F198A/S exhibited a τ_{off} of approximately 5.5±1.6/6.4±2.0 s, compared with 29±2.3 s for wild type (Fig. 3b, Table 1). The EC_{50} of IVM effect on potentiation and deactivation of F198A/S (EC_{50}=2.02±0.52/1.90±0.44 μM and 6.12±1.85/ 5.84±1.56 μM) showed rightward shift compared with wild type (EC_{50}=0.23±0.05 μM and 2.16±0.45 μM) (Fig. 3d and e, Table 2), indicating a reduced IVM potency. The equivalent F198A mutant of P2X$_1$ receptor resulted in half peak current amplitude with no significant change in the ATP potency compared with wild type [23]. This result was similar to the effect found for Val^{49} and Gly^{29} in transmembrane domains [24]. All these results implied that Tyr^{54}, Phe^{198}, and Trp^{259} played important roles in channel function as aromatic residues.

We next looked at the mutants that produced functional channels with normal ATP EC_{50} values, Y195A/S, F330A/S, and F200A/S, to see if they exhibited different sensitivities

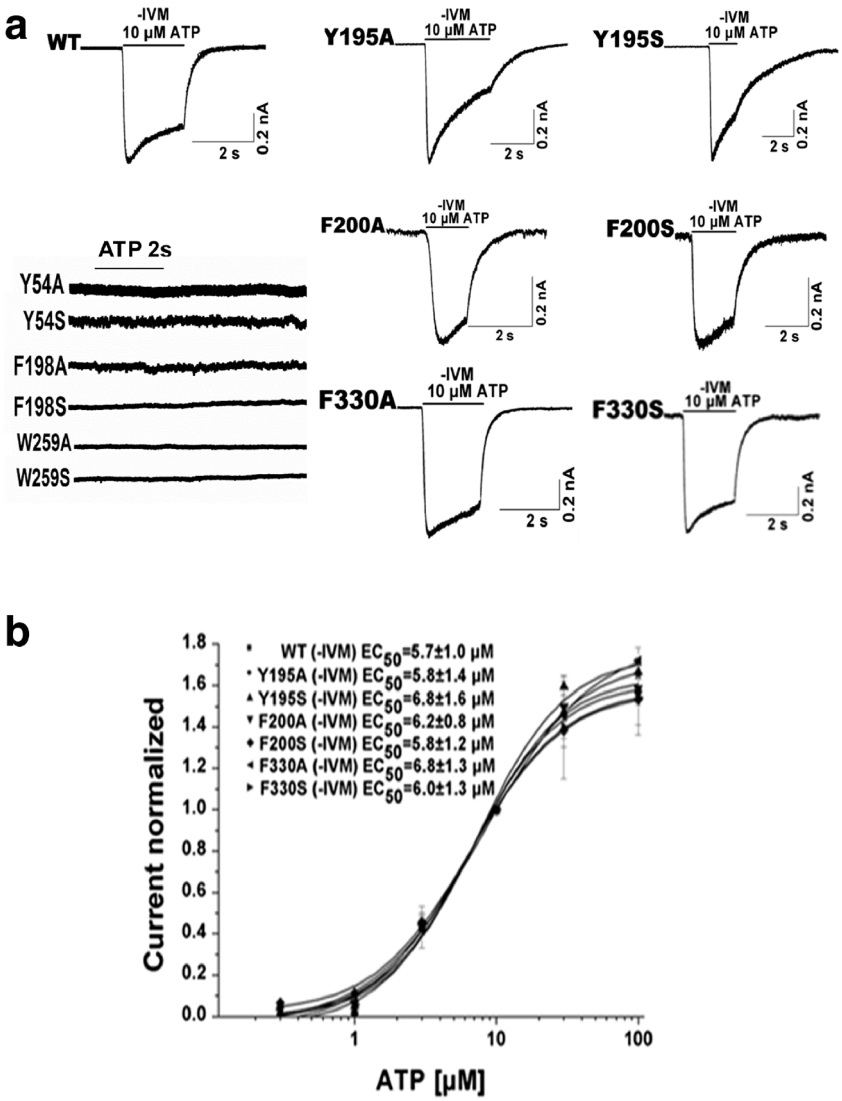

Fig. 2 The characterization of the wild-type and mutants of $P2X_4R$. **a** Trace recording of 1–3 mM ATP-induced currents for the Y54A/S, F198A/S, and W259A/S mutants and example records of 10 μM ATP-induced currents in the absence of IVM for the WT, Y195A/S, F200A/S, and F330A/S mutants. **b** Concentration–response curves of ATP for the WT (n=15) and the Y195A/S (n=8/7), F200A/S (n=6/4), and F330A/S mutants (n=6/5)

to allosteric modulation by IVM. In the presence of 3 μM IVM, the deactivation time constant was significantly prolonged for two mutants, Y195A/S (τ_{off}=51±2.4/54±1.2 s) and F330A/S (τ_{off}=40±4.9/47±4.5 s), and was reduced for F200A/S (τ_{off}=10±3.9/10±4.4 s) compared with the wild type (τ_{off}=29±2.3 s) (Table 1, Fig. 4a and b).

Given that Y195A/S, F330A/S, and F200A/S all had the same ATP sensitivities as the wild-type $P2X_4R$ (Fig. 2b, Table 1), two potential factors likely contributed to the prolonged or reduced decay time of the current during the washout of the agonist: (1) the mutant changed the IVM-binding properties and (2) the mutant changed the signal transduction mechanism by which bound IVM altered channel gating sensitivity to ATP. The concentration–response relationship for the effect of IVM on current reflected IVM potency for the receptor; the potency of IVM was a combined measure of the ability of IVM to bind to the receptor (affinity) and the subsequent functional opening of channel gating induced by agonist [23]. We respectively tested the EC_{50} of IVM on current amplitude and deactivation time activated by 10 μM ATP to evaluate the IVM-binding properties for receptor. Activated by ATP, the EC_{50} of IVM on current amplitude of F200A/S (EC_{50}=0.02±0.01/0.03±0.02 μM) leftward shifted while Y195A/S(EC_{50}=0.78±0.11/0.82±0.23 μM) rightward shifted compared with wild type (EC_{50}=0.23±0.05 μM), and F330A/S (EC_{50}=0.55±0.22/0.63±0.32 μM) showed comparable EC_{50} to wild type (Fig. 4c, Table 2). The EC_{50} of IVM on deactivation time of F200A/S (EC_{50}=4.28±1.88/4.86±1.62 μM), Y195A/S (EC_{50}=1.97±0.24/2.12±0.38 μM), and F330A/S (EC_{50}=1.90±0.44/2.08±0.28 μM) showed comparable values with wild type (EC_{50}=2.16±0.45 μM) (Fig. 4b, Table 2). As shown in Fig. 4, the IVM potency of the mutants and wild type did not change in parallel with the deactivation time. Obviously, the changed deactivation kinetics is not correlated with IVM-binding properties and reflects a change in the ability of bound IVM to alter gating function.

Table 1 Alanine- and serine-scanning mutagenesis of conserved large residues of the lateral fenestration domain of the $P2X_4$ receptor

Receptors	ATP EC_{50} (μM)	n_H	−IVM-I_{max} (nA)	−IVM-τ_{off} (s)	+IVM-I_{max} (nA)	+IVM-τ_{off} (s)	I_{max} (fold increase)	*N*
WT $P2X_4$	5.7±1.0	1.3±0.2	1.6±0.12	0.4±0.02	2.9±0.2	29±2.3	1.9±0.2	15
Y54A[a]	NF		NF	NF	NF	NF	NF	
Y54S[a]	NF		NF	NF	NF	NF	NF	
Y195A	5.8±1.4	1.4±0.3	0.7±0.1***	2.4±0.52**	1.7±0.2**	51±2.4***	2.4±0.1*	8
Y195S	6.8±1.6	1.0±0.1	0.5±0.2***	1.6±0.24***	1.2±0.4**	54±1.2***	2.2±0.1	7
F198A[b]	ND		ND	ND	0.9±0.3***	5.5±1.6***	ND	5
F198S[b]	ND		ND	ND	0.7±0.2***	6.4±2.0***	ND	5
F200A	6.2±0.8	1.7±0.4	1.0±0.5	0.7±0.07**	2.1±0.7	10±3.9**	2.3±0.5	6
F200S	5.8±1.2	1.5±0.3	1.2±0.2*	0.3±0.09	2.3±0.4	10±4.4**	2.0±0.1	4
W259A[b]	ND		ND	ND	0.05±0.02***	17±1.0**	ND	4
W259S[b]	ND		ND	ND	0.04±0.02***	16±3.0**	ND	4
F330A	6.8±1.3	1.6±0.4	1.3±0.3	0.4±0.10	2.5±0.5	40±4.9*	2.0±0.2	6
F330S	6.0±1.3	1.4±0.2	1.4±0.4	0.4±0.08	3.0±0.8	47±4.5**	2.1±0.2	5

Each receptor was examined in 4 to 15 cells in the presence (+IVM) or absence (−IVM) of 3 μM IVM, and the number of cells studied is given by *n*

NF non-functional mutants, *ND* non-determined mutants

[a] Mutant did not show function when the ATP concentration was increased to 3 mM

[b] ATP (1–3 mM) was used to estimate I_{max} in the absence of IVM

*$P<0.05$, **$P<0.01$, or ***$P<0.001$, respectively, denote significant differences from WT or WT with IVM

Taken together, these results provide further evidence that bulky side chains within the linker regions are critical to channel gating.

Discussion

The current study sought to investigate the influence on channel gating of several conserved aromatic side chain residues located near the lateral fenestrations of $P2X_4R$. We chose these residues because the positions they occupy also serve as part of the linker regions connecting the ATP-binding ectodomain of $P2X_4R$ with the pore-forming transmembrane domain. Zemkova reported the residues above TM1 were predominantly responsible for ion uptake into the extracellular vestibule lumen, whereas TM2 predominantly facilitated access to gate and permeation [25]. Molecular simulations were consistent with the prediction that the structure of these domains was important for conveying the conformational change caused by ATP binding to the gate-forming transmembrane helixes [26]. We report two principal findings. First, mutation of three residues, Tyr^{54}, Phe^{198}, and Trp^{259}, produced mutants that expressed normally in the plasma membrane of transfected HEK293 cells but that were unresponsive to ATP concentrations as high as 1–3 mM. Second, mutation of four of the amino acids, Tyr^{195}, Phe^{198}, Phe^{200}, and Phe^{330}, altered the ability for the allosteric modulator, ivermectin, to sensitize $P2X_4R$ to ATP.

The Tyr^{54} and Phe^{330} respectively proximal to the TM1 and TM2 are situated at the bottom of the lateral ion access portal. In contrast, the Tyr^{195}, Phe^{198}, Phe^{200}, and Trp^{259} are situated at the top segment of lateral portal (Fig. 1b). For P2XR, agonist-induced rotation of the propeller-head domain of the receptor, sliding of adjacent subunits leading to restricted access to the upper vestibule, movement in the ion-conducting lateral portals, and gating of the channel pore have been demonstrated [27].

Recently, Rokic conducted a similar study that focused on residues between Val^{47} and Val^{61} near the TM1 domain, and residues Phe^{324} to Asn^{338} near the TM2 domain. They identified five residues, Val^{49}, Tyr^{54}, Gln^{55}, Phe^{324}, and Gly^{325}, which yielded non-functional receptors when substituted with alanine [28]. With the exception of Val^{49}, which substantially impaired protein trafficking, these mutants were expressed in the plasma membrane of transfected HEK293 cells, and partial function could be recovered by IVM-mediated sensitization. Consistent with this previous work, we too observed that substitution of Tyr^{54} yielded a non-functional receptor that was nevertheless expressed in the plasma membrane, although, in our hands, we were not able to recover function with IVM. Mutation of Tyr^{55} of the rat $P2X_2R$, which is analogous to Tyr^{54} in $P2X_4R$, has also been reported to yield non-functional receptors [29].

We identified two additional aromatic side chains within the linker regions of $P2X_4R$, Phe^{198}, and Trp^{259}, which also rendered $P2X_4R$ non-functional when mutated. Alanine substitutions at analogous positions in $P2X_1R$ also yielded non-functional mutants. In the case of Phe^{198}, this appeared to be due to an impairment of channel gating, and our data for this position in $P2X_4R$ supported this [23]. Indeed, we were able to

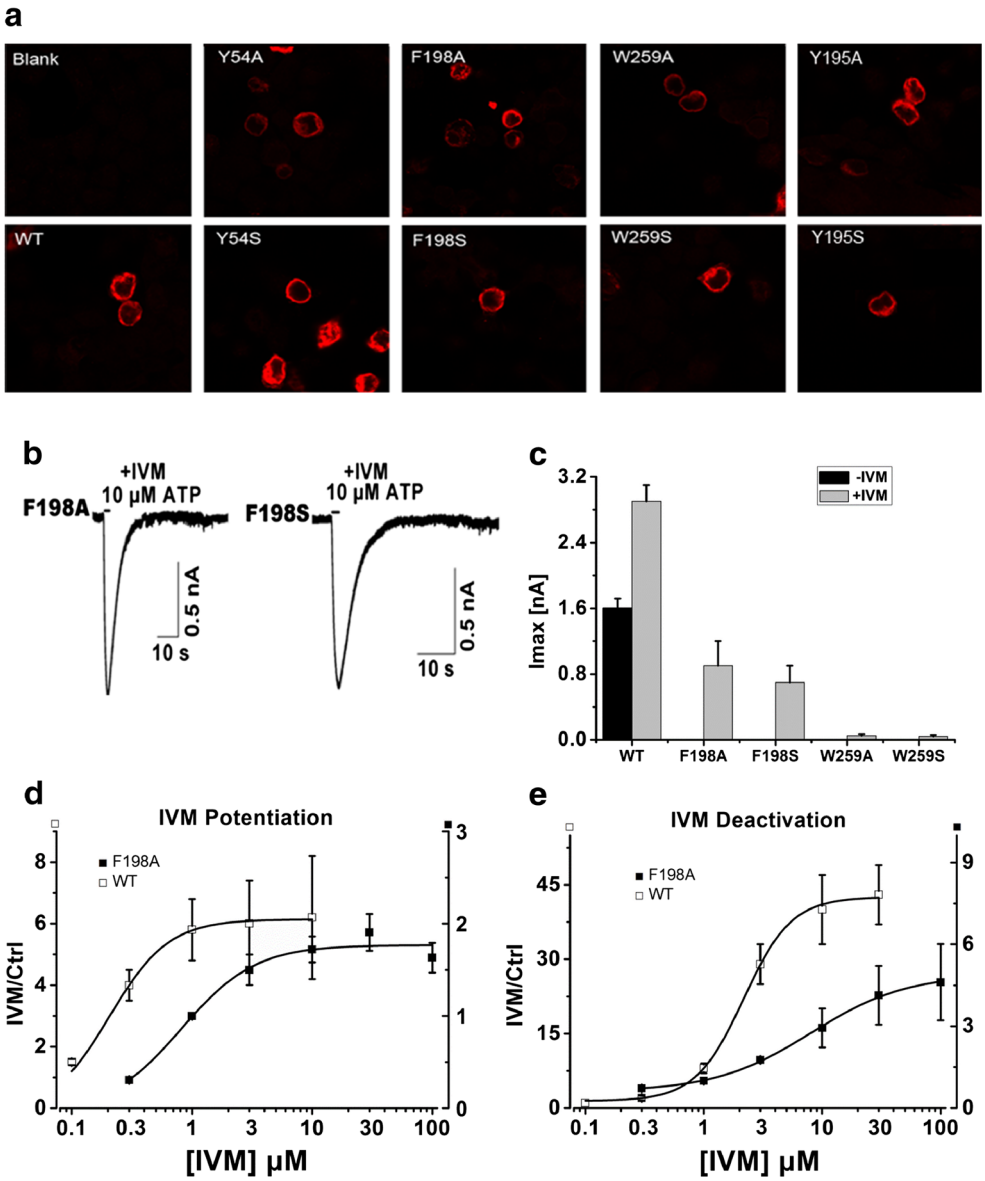

Fig. 3 The characterization of the substitution-deficient mutants of $P2X_4R$. **a** The expression pattern of WT and Y195A/S, Y54A/S, F198A/S, and W259A/S mutants in HEK293 cells, examined by laser-scanning confocal microscopy (three experiments). **b** The effects of 3 μM IVM on the 10 μM ATP-induced current in HEK293 cells expressing the F198A/S mutants. **c** The augmentation of the maximum current amplitude of the WT (n=15), F198A/S (n=5/5), and W259A/S (n=4/4) by 3 μM IVM. **d** Concentration–response curves of IVM potentiation for the WT (n=10) and F198A (n=6) receptor. (**e**). Concentration–response curves of IVM deactivation for the WT (n=10) and F198A (n=6) receptor

Table 2 IVM potency of wild-type and mutant receptors

Receptors	IVM potentiation EC_{50} (μM)	n_H	IVM deactivation EC_{50} (μM)	n_H	n
WT $P2X_4$	0.23±0.05	1.8±0.2	2.16±0.45	2.1±0.4	10
Y195A	0.78±0.11**	1.7±0.3	1.97±0.24	2.2±0.5	6
Y195S	0.82±0.23*	2.1±0.3	2.12±0.38	2.4±0.4	7
F198A	2.02±0.52**	2.1±0.2	6.12±1.85**	2.3±0.1	6
F198S	1.90±0.44**	1.4±0.4	5.84±1.56*	1.8±0.1	6
F200A	0.02±0.01**	1.1±0.3	4.28±1.88	1.4±0.3	7
F200S	0.03±0.02**	1.2±0.2	4.86±1.62*	1.5±0.3	5
F330A	0.55±0.22	1.8±0.3	1.90±0.44	2.4±0.2	5
F330S	0.63±0.32	1.7±0.4	2.08±0.28	2.1±0.3	6

Each receptor was examined in five to ten cells in the presence IVM, and the number of cells studied is given by n are denoted with*P<0.05, or **P<0.01, respectively, denote significant differences from WT with IVM

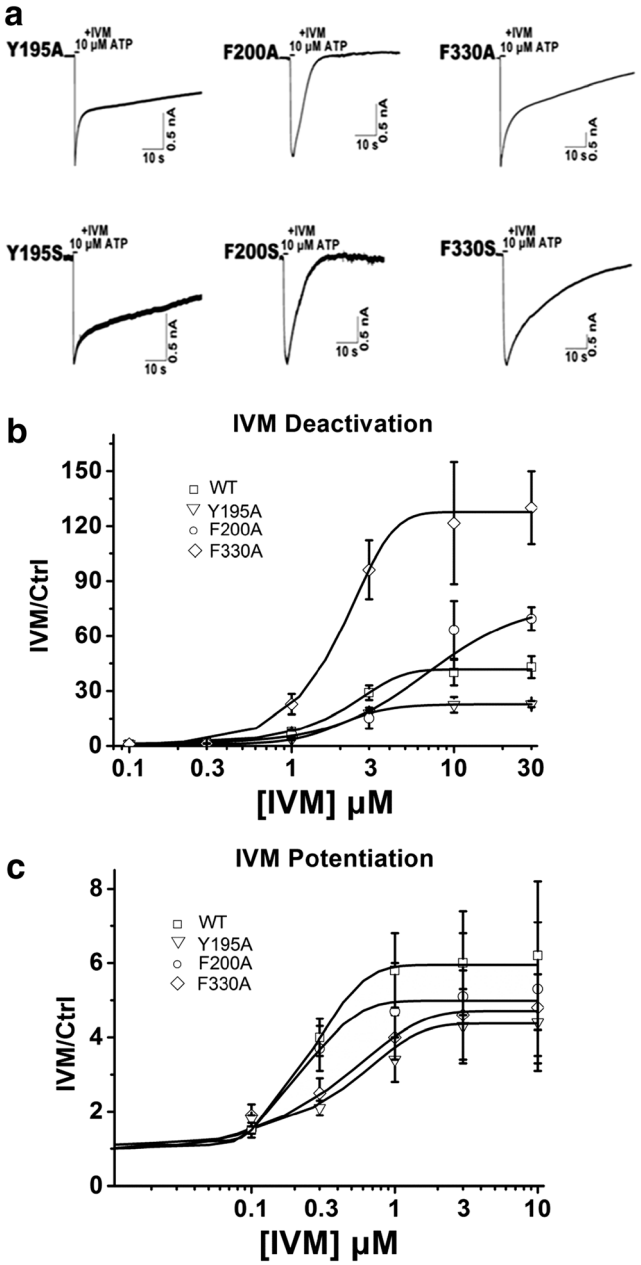

Fig. 4 The characterization of the substitution-normal mutants of $P2X_4R$. **a** Example records of 10 μM ATP-induced currents in the presence of 3 μM IVM for the Y195A/S, F200A/S, and F330A/S mutants. **b** Concentration–response curves of IVM deactivation for the WT (n=10), Y195A (n=6), F200A (n=7), and F330A (n=5) receptor. **c** Concentration–response curves of IVM potentiation for the WT (n=10), Y195A (n=6), F200A (n=7), and F330A (n=5) receptor

show in this paper that the ATP-gated current functionality of Phe^{198} mutants could be recovered in IVM. In contrast to our immunofluorescence data for $P2X_4R$-W259A, the analogous mutation in $P2X_1$ yielded receptors that were not functionally expressed in the plasma membrane [23], and Nakazawa reported an aromatic ring with a hydroxyl group was necessary exactly at position 256 for $P2X_2R$ activation [30]. We reported here that volume was critical for the linker region residues contributing to the receptor function. The mutants of Tyr^{54} were entirely nonfunctional and could not be rescued by IVM. It was reasonable to speculate that this residue was critical for channel-gating. In the study of molecular dynamics simulations of the $P2X_4R$, the Tyr^{54} residue could form interactions with the Phe^{48} and Phe^{330}, and the interactions were important for channel-gating. We did the experiments of mutants of Phe^{330} and found that Phe^{330} was not a key point for channel function. Our results showed that the distance between Tyr^{54} and Phe^{48} was short; the hydroxyl groups of Tyr^{54} and Phe^{48} could form strong interaction. Distance was critical for this interaction contributing to the channel-gating (Fig. 5a). As shown in Fig. 5b, Arg^{203} was a critical residue for ATP-binding or channel-gating; this residue was involved in

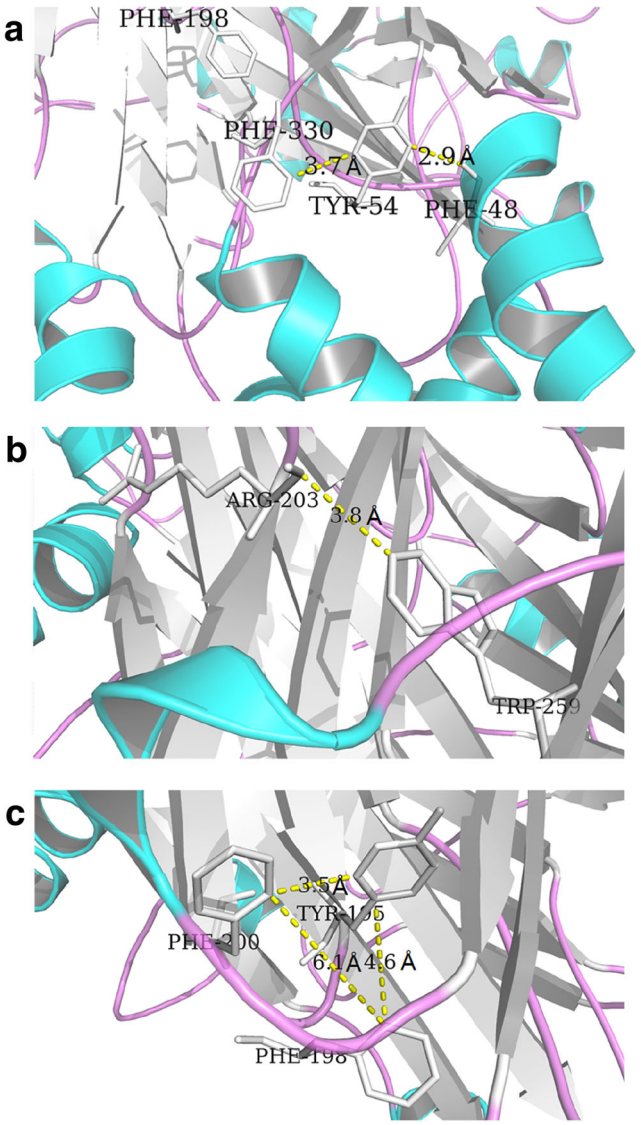

Fig. 5 The possible roles of Tyr^{54}, Trp^{259}, and Phe^{198} played in $P2X_4R$. **a** Residue Tyr^{54} can form strong interaction with Phe^{48}. **b** Trp^{259} can form stacking interaction with Arg^{203}. **c** Phe^{198}, Tyr^{195}, and Phe^{200} can form a random coil, and Phe^{198} locates at the corner in the coil

interactions between the left flipper and lower body domains [31, 32]. The distance between Arg^{203} and Trp^{259} was short enough for an interaction; the hydroxyl group of Trp^{259} and the guanidyl group of Arg^{203} could form strong interaction. Trp^{259} affected the channel function by the interaction with Arg^{203} (Fig. 5b). Phe^{198}, Tyr^{195}, and Phe^{200} formed a random coil (Fig. 5c); this random coil could influence the function of the receptor. Phe^{198} located in the corner of this random coil, so this residue was more important than the other two residues as shown in our results in channel function.

Substitutions introduced at three other positions, Tyr^{195}, Phe^{200}, and Phe^{330}, produced functional receptors with normal ATP EC_{50} values. Whereas the current profiles for F200A/S and F330A/S mutants were similar to wild type, the time course for current deactivation through Y195A/S mutants was significantly prolonged, possibly indicative of gating effects (Fig. 2a, Table 1). Furthermore, substitution of these residues was found to have a more nuanced impact on channel gating largely by altering the sensitivity of $P2X_4R$ to allosteric modulation by IVM. IVM is known to modulate $P2X_4R$ function in two specific ways [13], possibly as a result of IVM interacting with two independent high- and low-affinity sites [33]. The high affinity effect of IVM is manifest as a potentiation in the amplitude of the ATP-gated current, whereas the low affinity effect is manifest as a prolongation of the time course for current deactivation upon ATP washout. Zemkova regarded the two different effects as IVM had distinct effects on opening and dilation of the channel pore, the first accounting for increased peak current amplitude and the latter correlating with changes in the EC_{50} and kinetics of deactivation [34]. We had reservations because Khakh concluded that IVM did not change the open state of $P2X_4R$ [13]. Previous work on understanding how IVM facilitates the function of $P2X_4R$ has strongly favored a role for the TM domains in forming the binding sites for IVM, which makes sense given the propensity of this drug to partition into the lipid bilayer [24, 31, 35]. Single-channel analysis revealed that IVM binding altered gating by stabilizing the open conformation of the channel, thereby increasing open probability in the presence of ATP [33]. We observed that alanine and serine mutations introduced at four positions, Tyr^{195}, Phe^{198}, Phe^{200} and Phe^{330}, substantially altered the ability for IVM to prolong ATP-gated current deactivation. The facilitating effect of IVM on $P2X_4R$ varied when incubated with different concentrations of IVM.

In the case of Y195A/S, the fold increase in time course of current deactivation in the presence of IVM was reduced relative to wild type, although this was likely due to the fact that this mutation increased the deactivation time-course of ATP-currents in the absence of IVM, thus potentially decreasing the fold-range over which IVM exerted an effect. Mutation of Phe^{330} substantially augmented the effect of IVM on current deactivation, whereas mutation of residues, Phe^{198} and Phe^{200}, significantly attenuated this aspect of IVM sensitivity. Consistent with these changes likely not affecting IVM binding to the low affinity site per se, the half-maximal concentrations of IVM required to influence either ATP-gated current deactivation were not substantially different for the mutants compared to wild-type $P2X_4R$. Thus, we believe that, while IVM likely binds the TM domains, its impact on ATP gating is in part determined by critical signal transduction residues in the linker regions connecting the ligand-binding and pore-forming domains.

In summary, we present data supporting an important signal transduction/gating role for conserved aromatic residues located within regions of peptide linking the ATP-binding ectodomain of $P2X_4R$ to its pore-forming transmembrane domain. In addition to being important for normal ATP gating of $P2X_4R$, our data suggest that these positions also influence the mechanism by which bound IVM allosterically modulates the ability for ATP to induce the necessary conformational changes associated with channel opening.

Acknowledgments We are grateful to Prof. Terrance M. Egan for providing the $P2X_4$ plasmid.

This study was supported by the National Natural Science Foundation of China (81171037/H0903) and the National Key Basic Research Program of China (973 Program) (2012CB966400).

Conflict of interest The authors declare that they have no conflict of interest.

Authorship contributions Participated in Research design: Gao, Li.
Conducted experiments: Gao, Yu.
Contributed new reagents or analytic tools: Xu, Zhang, Ma.
Performed data analysis: Liu, Jie.
Wrote or contributed to the writing of the manuscript: Gao, Samways, Li.

References

1. Surprenant A, Buell G, North RA (1995) P2X receptors bring new structure to ligand-gated ion channels. Trends Neurosci 18:224–229
2. Newbolt A, Stoop R, Virginio C, Surprenant A, North RA, Buell G, Rassendren F (1998) Membrane topology of an ATP-gated ion channel (P2X receptor). J Biol Chem 273:15177–15182
3. Shrivastava AN, Triller A, Sieghart W, Sarto-Jackson I (2011) Regulation of GABA(A) receptor dynamics by interaction with purinergic P2X(2) receptors. J Biol Chem 286:14455–14468
4. Evans RJ, Derkach V, Surprenant A (1992) ATP mediates fast synaptic transmission in mammalian neurons. Nature 357:503–505
5. Migita K, Haines WR, Voigt MM, Egan TM (2001) Polar residues of the second transmembrane domain influence cation permeability of the ATP-gated P2X(2) receptor. J Biol Chem 276:30934–30941
6. Gu JG, MacDermott AB (1997) Activation of ATP P2X receptors elicits glutamate release from sensory neuron synapses. Nature 389:749–753
7. Khakh BS, Henderson G (1998) ATP receptor-mediated enhancement of fast excitatory neurotransmitter release in the brain. Mol Pharmacol 54:372–378

8. Shatarat A, Dunn WR, Ralevic V (2014) Raised tone reveals ATP as a sympathetic neurotransmitter in the porcine mesenteric arterial bed. Purinergic Signalling 10:639–649
9. Buell G, Lewis C, Collo G, North RA, Surprenant A (1996) An antagonist-insensitive P2X receptor expressed in epithelia and brain. Embo J 15:55–62
10. Seguela P, Haghighi A, Soghomonian JJ, Cooper E (1996) A novel neuronal P2x ATP receptor ion channel with widespread distribution in the brain. J Neurosci 16:448–455
11. Li GH, Lee EM, Blair D, Holding C, Poronnik P, Cook DI, Barden JA, Bennett MR (2000) The distribution of P2X receptor clusters on individual neurons in sympathetic ganglia and their redistribution on agonist activation. J Biol Chem 275:29107–29112
12. Burnstock G (2014) Purinergic signalling in endocrine organs. Purinergic Signalling 10:189–231
13. Khakh BS, Proctor WR, Dunwiddie TV, Labarca C, Lester HA (1999) Allosteric control of gating and kinetics at P2X(4) receptor channels. J Neurosci 19:7289–7299
14. Norenberg W, Sobottka H, Hempel C, Plotz T, Fischer W, Schmalzing G, Schaefer M (2012) Positive allosteric modulation by ivermectin of human but not murine P2X7 receptors. Br J Pharmacol 167:48–66
15. Ejere H, Schwartz E, Wormald R (2001) Ivermectin for onchocercal eye disease (river blindness). The Cochrane Database Syst Rev 1, CD002219
16. Dent JA, Davis MW, Avery L (1997) avr-15 encodes a chloride channel subunit that mediates inhibitory glutamatergic neurotransmission and ivermectin sensitivity in *Caenorhabditis elegans*. Embo J 16:5867–5879
17. Kawate T, Michel JC, Birdsong WT, Gouaux E (2009) Crystal structure of the ATP-gated P2X(4) ion channel in the closed state. Nature 460:592–598
18. Samways DSK, Khakh BS, Egan TM (2012) Allosteric modulation of Ca^{2+} flux in ligand-gated cation channel (P2X4) by actions on lateral portals. J Biol Chem 287:7594–7602
19. Samways DSK, Khakh BS, Dutertre S, Egan TM (2011) Preferential use of unobstructed lateral portals as the access route to the pore of human ATP-gated ion channels (P2X receptors). Proc Natl Acad Sci U S A 108:13800–13805
20. Kracun S, Chaptal V, Abramson J, Khakh BS (2010) Gated access to the pore of a P2X receptor: structural implications for closed–open transitions. J Biol Chem 285:10110–21
21. Kawate T, Robertson JL, Li M, Silberberg SD, Swartz KJ (2011) Ion access pathway to the transmembrane pore in P2X receptor channels. J Gen Physiol 137:579–90
22. Jelinkova I, Yan ZH, Liang ZD, Moonat S, Teisinger J, Stojilkovic SS, Zemkova H (2006) Identification of P2X4 receptor-specific residues contributing to the ivermectin effects on channel deactivation. Biochem Biophys Res Commun 349:619–625
23. Roberts JA, Evans RJ (2004) ATP binding at human P2X1 receptors. Contribution of aromatic and basic amino acids revealed using mutagenesis and partial agonists. J Biol Chem 279:9043–55
24. Zemkova H, Jelinkova I, Vavra V, Jindrichova M, Obsil T, Zemkova HW, Stojilkovic SS (2008) Identification of P2X(4) receptor transmembrane residues contributing to channel gating and interaction with ivermectin. Pflugers Arch Eur J Physiol 456:939–950
25. Rokic MB, Stojilkovic SS, Zemkova H (2014) Structural and functional properties of the rat P2X4 purinoreceptor extracellular vestibule during gating. Front Cell Neurosci. doi:10.3389/fncel.2014.00003
26. Du J, Dong H, Zhou HX (2012) Gating mechanism of a P2X4 receptor developed from normal mode analysis and molecular dynamics simulations. Proc Natl Acad Sci U S A 109:4140–5
27. Roberts JA, Allsopp RC, El Ajouz S, Vial C, Schmid R, Young MT, Evans RJ (2012) Agonist binding evokes extensive conformational changes in the extracellular domain of the ATP-gated human P2X1 receptor ion channel. Proc Natl Acad Sci U S A 109:4663–4667
28. Rokic MB, Stojilkovic SS, Vavra V, Kuzyk P, Tvrdonova V, Zemkova H (2013) Multiple roles of the extracellular vestibule amino acid residues in the function of the rat P2X4 receptor. PloS One 8:e59411
29. Jiang LH, Rassendren F, Spelta V, Surprenant A, North RA (2001) Amino acid residues involved in gating identified in the first membrane-spanning domain of the rat P2X(2) receptor. J Biol Chem 276:14902–8
30. Nakazawa K, Sawa H, Ojima H, Ishii-Nozawa R, Takeuchi K, Ohno Y (2002) Size of side-chain at channel pore mouth affects $Ca^{(2+)}$ block of P2X(2) receptor. Eur J Pharmacol 449:207–11
31. Hattori M, Gouaux E (2012) Molecular mechanism of ATP binding and ion channel activation in P2X receptors. Nature 485:207–212
32. Tvrdonova V, Rokic MB, Stojilkovic SS, Zemkova H (2014) Identification of functionally important residues of the rat P2X4 receptor by alanine scanning mutagenesis of the dorsal fin and left flipper domains. PloS One 9:e112902
33. Priel A, Silberberg SD (2004) Mechanism of ivermectin facilitation of human P2X4 receptor channels. J Gen Physiol 123:281–293
34. Zemkova H, Khadra A, Rokic MB, Tvrdonova V, Sherman A, Stojilkovic SS (2014) Allosteric regulation of the P2X4 receptor channel pore dilation. Arch Eur J Physiol. doi:10.1007/s00424-014-1546-7
35. Silberberg SD, Li MF, Swartz KJ (2007) Ivermectin interaction with transmembrane helices reveals widespread rearrangements during opening of P2X receptor channels. Neuron 54:263–274